Montana Bureau of Mines and Geology

PROCEEDINGS

Berkeley and Continental pits. Photo by Mark Thompson, Montana Resources.

Montana Mining and Mineral Symposium 2018
October 9–October 11, 2019
Montana Bureau of Mines and Geology
Special Publication 121

Supporting the Transition to Deep Porphyry Copper Exploration: SHRIMP U/Pb Radiometric Dating of Titanite ($CaTiSiO_5$) in the Distal and Superjacent Orbicular Alteration Zone of the Clementine Prospect, Southwest Montana

George Brimhall[1] and Mark Fanning[2]

[1]*Clementine Exploration, Wise River, Montana*

[2]*Arise Geosciences Pty Ltd, Australian National University, Canberra ACT, Australia*

Abstract

The projected increase in world requirements for copper, even considering recycling, will require mining more copper over the next three decades than was mined in all prior human history. Since there are no good substitutes for copper's ubiquitous electrical uses, the failure over the past decade to discover more than a few new shallow porphyry copper deposits (PCD) and some near-mine, brownfields discoveries, a pressing need exists for a decisive change in how the search for new deeper orebodies is designed and prospects are scientifically evaluated. This is a daunting challenge as many ore bodies with their tops located 1 km or more below surface are unlikely to exhibit the traditional signs on the surface that have guided past exploration, which applied the extant porphyry copper genetic paradigm. The intent of this work on orbicular alteration is revising the distal and upper reaches of the geo-spatial patterns of the PCD paradigm and providing new field methods that help support the transition to deep PCD exploration. First, exploring through the tops of prospective new deep porphyry copper deposits means confronting the realities of a largely unfamiliar geological domain above the current tops of the porphyry copper paradigms, based on mined ore deposits whose surface exposures intersected the surface within ore grade levels. Deeper targets are different in that their tops are 500 to 1,000 m above ore grade levels. This report describes our efforts on the Clementine prospect to extend the porphyry copper paradigm upwards to include the tops of potential deep orebodies, where their distal wall rock alteration is likely to be encountered first in exploration as the outermost ring of concentric features. We describe low-grade disseminated chalcopyrite zones within orbicular alteration zones representing a cupola at the upper and outer edge of hydro-fractured stockworks where advective flow slowed and spherical actinolite-calcite-titanite orbs formed by diffusion under low chemical Peclet Number conditions. Orb alteration makes this subtle physical boundary feature macroscopically visible and contributes a powerful new mapping tool in lithologies where orbs are likely to form as in sedimentary and other wall rocks with connected pore space, allowing intergranular diffusion, rather than in non-porous rocks with interlocking grains. Nevertheless, we have observed and mapped orbs in gabbro sills. In comparison to strongly advective flow vein systems with planar, vein-parallel wall rock alteration zones like Mainstage Butte veins, distal orb growth involved alteration fronts that are functionally wrapped into 1- to 3-cm-diameter spheres at crack tips forming nested semi-spherical reaction fronts that slowly migrated outwards, with inner reaction fronts replacing outer fronts. In order to determine the age of the hydrothermal titanite, we used *in situ* ion probe methods in which single grains offer multiple independent analysis spots. Using the Tera-Wasserburg plotting method, we determined a U/Pb SHRIMP date of hydrothermal titanite of 70.7 million years, which is similar to the plutonic age range of the Boulder and Pioneer Batholiths, thus eliminating concern that orbs are merely a strange regional metamorphic effect. Similarly, this new age date supports the hydrothermal origin of the orbs that alter many different rock formations and are axially-symmetrically aligned with respect to vein gossans, breccias, and felsic plutons at the center of the zoning pattern. Furthermore, the normality of orbicular alteration within the PCD model is further established by describing the close geochemical conditions of the titanite-ilmenite-chalcopyrite assemblage with potassic biotite-bearing alteration and early high-temperature mineralization. Orb mapping and radiometric dating of titanite can assist in targeting large, deep porphyry copper deposits during early exploration through properly interpreting the orbicular zonation surrounding the typical alteration halo around large intrusive systems as the exterior of the system's fracture pattern, thus providing a bullseye to focus follow up exploration. Our approach offers new unequivocal

geological evidence that may prove more trustworthy in discerning the large, deep chalcopyrite-bornite PCD targets than amassing a host of conventional geochemical data on late vein systems that can be offset from the early stage mineralization.

Introduction

Axially symmetric vein gossans, breccias, and felsic plutons surrounded by distal actinolite-calcite-titanite-filled orbicular alteration with disseminated pyrrhotite, chalcopyrite, and ilmenite between orbs were described by Brimhall at the Clementine prospect of southwest Montana (Brimhall, 2018). The Clementine system was interpreted as the top of a possible deep porphyry copper deposit (PCD) emplaced with clear regional structural control near the axial crest of a doubly plunging anticline (fig. 1), confined by the overlying Grasshopper thrust plate. Brimhall (2018) interpreted the orbs in plan and cross section as describing a cupola formed at the outer and upper edge of hydro-fractured stockworks. Here, the advective flow rate slowed considerably at the fringes of the magmatically heated convective system such that spherical hydrothermal orbs formed by in situ diffusion from the outermost and uppermost crack tips or crack intersections as aqueous ions migrated over short distances after arriving at this distal position by convective fluid flow. Using the chemical Peclet number, which describes the relative importance of advective transport and diffusion in a continuum, Brimhall (2018) showed that the orb zones define the advective/diffusive boundary of a large hydrothermal system 2 by 6 km centered on the vein gossans, breccias, and felsic plutons. The utility of orb cupolas as a targeting tool in PCD exploration then stems from the assertion that orbicular zones mark the position of a key hydrodynamic boundary: the peripheral edge of the mineralized fracture permeability network at the time of coupled wall rock alteration and copper mineralization, since disseminated chalcopyrite occurs in the rock matrix between the orbs. Orb alteration makes this subtle physical boundary feature macroscopically visible and contributes a powerful new mapping tool in lithologies where orbs are likely to form in sedimentary and other rocks with connected pore space, allowing intergranular diffusion, rather than in non-porous rocks with interlocking grains. The orbicular alteration described in Brimhall (2018) was viewed as an innovation that can assist targeting large, deep porphyry copper deposits during early exploration through properly interpreting the orbicular zonation surrounding the typical alteration halo around these large intrusive systems as the exterior of the system's fracture pattern, providing a bullseye to focus follow-up exploration (Shaffer, 2019). Similarly, since it has now been shown at the Clementine prospect that springs today occur near the orb bands (fig. 1), it is inferred that the gross permeability of the hornfels altered rocks inside the orb cupola is lower than those outside the cupola in unaltered formations. Hence, the spatial association of springs with orb bands provide another exploration tool of using mapped springs from U.S. Geological Survey topographic maps to: (1) help find and map orbicular alteration and associated disseminated sulfide mineralization in new districts, and (2) infer on a potential district scale, the position, size, and orientation of a new prospective region of interest.

The Clementine zonation pattern is the first complete geologically mapped orbicular actinolite alteration cupola since such alteration was first described in logged diamond drill core from the contact metamorphic aureole at Carr Fork, Bingham, Utah (Atkinson and Einaudi, 1978) over 40 years ago. Since their insightful descriptions of orbs, orbs have been described, though not mapped, at three deposits in Chile: Caspiche, La Escondida, and El Hueso (Sillitoe and others, 2013); Cajamarca in Peru; Morenci and Fortitude Copper Canyon in the U.S.; Cananea in Mexico; and Oyu Tolgoi in Mongolia (Marco Einaudi, written commun., 2019). During the past four decades, opportunities to discover shallow porphyry copper orebodies have diminished significantly throughout much of the world (Wood, 2016), as reflected in the falling discovery rate of major orebodies from the early 1970s onward, while expenditures have continued to rise (Schodde, 2013). Sillitoe and others (2016) summarized the current discovery climate using traditional methods and the application of the Sillitoe (2010) porphyry copper deposit model: "in the past decade, deep exploration for porphyry copper deposits completely concealed beneath extensive lithocaps has become increasingly common as near-surface mineralization becomes scarcer, but with rare exceptions there have been few successes." Wood and Hedenquist (2019) go further in stating that overall, "exploration efforts since 2010 have been wealth destructive." Consequently, a compelling need exists to embrace deep exploration (Schodde, 2013) rather than continuing a traditional surface to near-surface target approach searching for exposed ore bodies. However, deeper ore bodies with their tops located 500 to 1,000

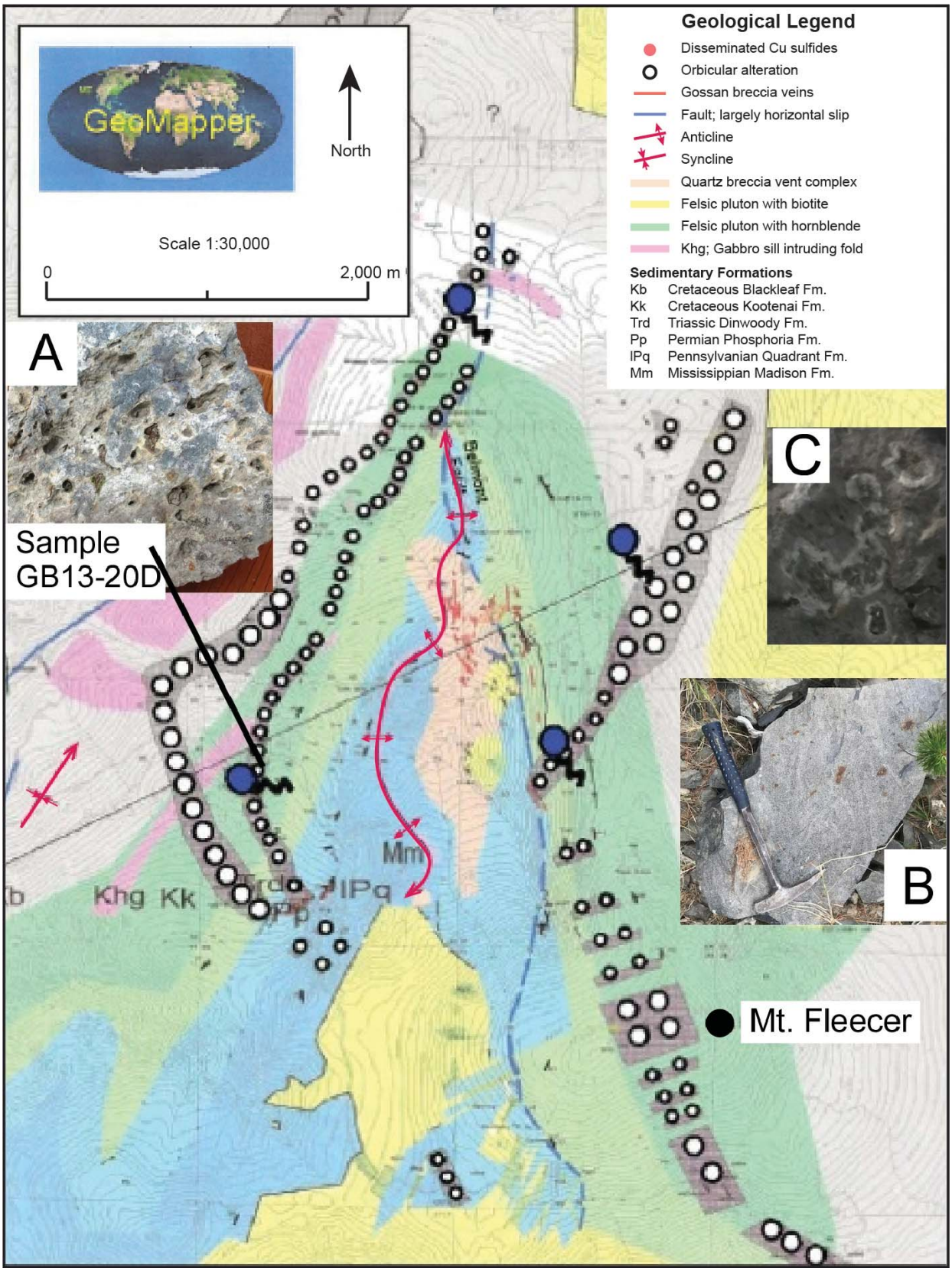

Figure 1. Bedrock geological plan map of Clementine (Brimhall, 2018). Formation abbreviations are: Mm (Mississippian Madison), lPq (Pennsylvanian Quadrant), Trd (Triassic Dinwoody), Kk (Cretaceous Kootenai), Khg (hornblende gabbro sills), and Kb (Cretaceous Blackleaf). Four groundwater-derived springs are shown with blue circles. (A) The orbicular alteration sampled for analysis in this study (sample GB13-20D). Mapping this alteration zone is possible largely due to four factors: (1) the surficial chemical weathering of the orbs where minerals are leached out, leaving vacuous cavities etched on exposed rock surfaces that are readily recognized while mapping; (2) the silicified nature of the alteration makes these rocks outcrop even under dense tree canopy; (3) the fact that disseminated pyrrhotite and ilmenite with ferrous iron oxidize and leave a rust-like ferric oxide surface coating (B); and (4) the orbs are often surrounded by white rings where biotite in the surrounding hornfels has been removed during orb growth diffusion (C).

m or more below surface are unlikely to exhibit the obvious signs on the surface which for decades was based on comparing new prospect mapping with models published by Lowell and Guilbert (1970) and Gustafson and Hunt (1975) on outcropping ore bodies exposed at their midsection levels, not their tops nor upper edges relevant now to deep exploration (John and others, 2010). In contrast, the orbicular cupola discovered and mapped at Clementine may prove useful in helping to fill in the nature and architecture of the vertical gap between the top of current porphyry copper paradigm (Sillitoe, 2010) and the superjacent region that is now the prime prospective region: the tops of deep porphyry copper deposits thus rendering this frontier less prone to misinterpretation and misallocation of exploration resources. The focus here is on helping to illuminate the unfamiliar superjacent zone through fieldwork and laboratory analysis. The work described here seeks to further demonstrate that orbicular alteration is indeed an integral part of porphyry copper alteration and not a mere petrological rarity, nor are orbs a strange metamorphic effect entirely unrelated to mineralization processes. Similarly, it is vital to not confuse actinolite-calcite-titanite orbs with orbicular granites, as the processes of formation are fundamentally different: fracture and diffusion-controlled hydrothermal alteration in contrast to solidification of magma.

With the regional geological patterns now described (fig. 1) proving the epigenetic hydrothermal origin of the orbs that crosscut and alter many different rock formations (Blackleaf, Kootenai, Dinwoody, Phosphoria, Quadrant, and gabbroic sills) and are axially-symmetrically aligned with respect to vein gossans, breccias, and felsic plutons, the goal here is to provide unequivocal answers to a key question at the pre-pilot drilling phase of exploration, specifically: What is the age of the orbicular actinolite-calcite-titanite alteration-disseminated chalcopyrite mineralization? Since junior exploration companies are expected to account for about 70 percent of porphyry copper discoveries over the next few decades (Schaffer, 2018) and the high cost of deep pilot hole drilling usually requires co-investment by larger mining companies, establishing the age of the mapped orb zones may help further understanding of the superjacent zone and perhaps motivate partnerships with major corporations. Towards that end, we intend that by radiometrically dating the orbs, we can demonstrate that orbicular alteration is in fact clearly related to axially-symmetric vein gossans, breccias, and felsic plutons surrounded by distal actinolite-calcite-titanite-filled orbicular alteration and can thus enhance the efficacy of the porphyry-copper paradigm used in exploration. Ideally, an orb ring would appear circular in plan view like a bullseye target. However, with the strong structural anticlinal control at Clementine, the bullseye is flattened into an ellipse.

Regional Geological Context

The Clementine prospect is shown in figure 2A in relation to well-known regional structures of the western U.S. comprising the ancient southwest Laurentia continent and major ore deposits including Butte, Bingham, Tintic, Henderson, and Questa (Pettke and others, 2010). Within the regional context that is believed to have influenced its formation and geochemical character, the Clementine prospect may represent the top of a new deep porphyry copper deposit situated at the intersection of the Great Falls and the Farmington tectonic zones, which are Proterozoic accretionary tectonic suture zones formed where early Proterozoic subduction zones and ancient oceans closed as the continental fragments coalesced and Laurentia (North America) was assembled. The Great Falls tectonic zone then originated at a convergent margin that developed during the closure of an ocean basin along the northwestern margin of the Wyoming craton ca. 1.9 Ga (Mueller and others, 2002). Today, much of the evidence of these ancient rocks is buried beneath Phanerozoic cover.

Clementine also occurs within the frontal fold of the Sevier Fold and Thrust Belt (fig. 2B) along the crest of a doubly plunging regional anticline that also contains the older mining districts and ore deposits at Quartz Hill, Cannivan Gulch, Hecla, and Argenta (fig. 2C). Along this north–south-trending anticlinorium, Clementine, Quartz Hill, and Hecla occur at doubly plunging anticlines or domes, revealing a clear local structural control in addition to the large-scale structures along which the parental magmas came up from depth.

A vertical cross section through Clementine is shown in figure 3. Our interpretation asserts that in southwestern Montana similar thrust sheet anticlines were the loci of magma ascent (Kalakay and others, 2001), mineralization, and alteration processes in syncompressional environments at the top of frontal thrust ramps

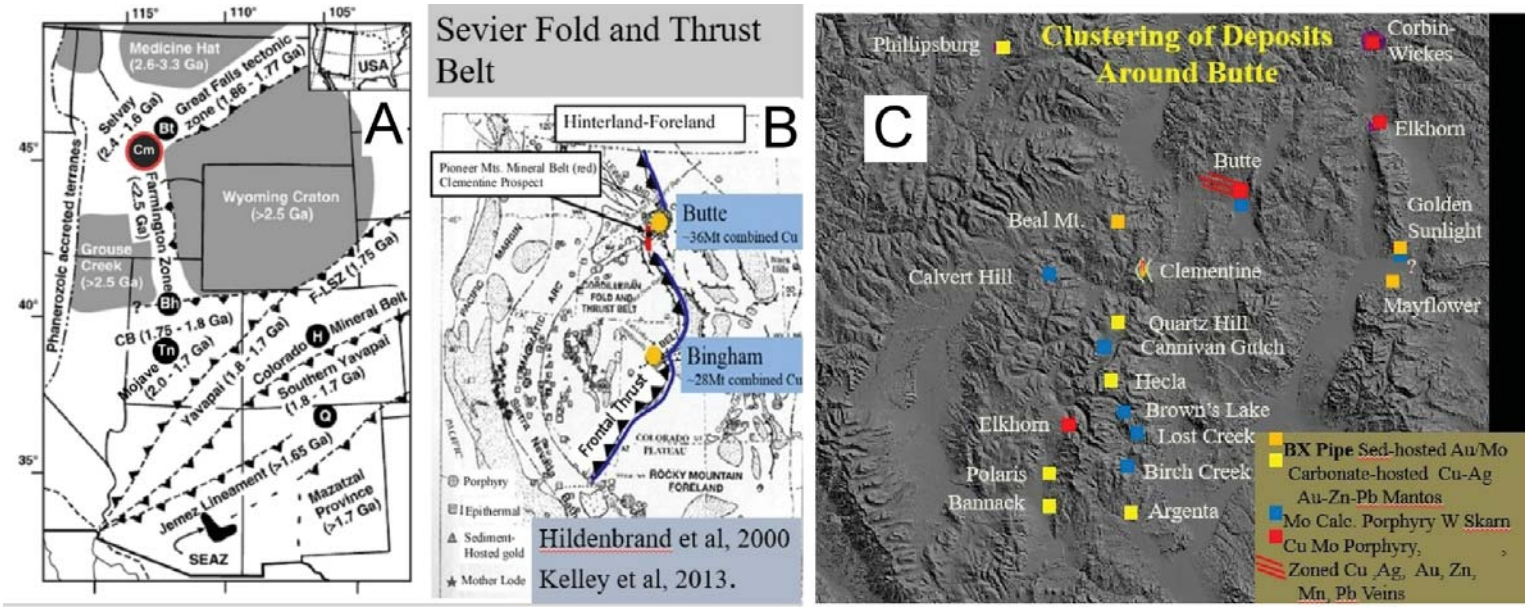

Figure 2. (A) Sketch of SW Laurentia (W USA) identifying major crustal segments (modified from Karlstrom and others, 2004; Foster and others, 2006). Archean crustal blocks (gray) are delimited by Proterozoic accretionary tectonic zones. Segments to the south of the Cheyenne Belt (CB) are terranes accreted during assembly of Laurentia, and sutures represent early Proterozoic subduction zones. The dash-dotted line separates terranes accreted to the Laurentian crustal block in the Phanerozoic. Filled black circles denote Clementine (Cm), Bingham (Bh), situated on the Uinta Axis, Butte (Bt), Henderson (H) in the Colorado Mineral Belt, Questa (Q) on the eastern rim of the Cenozoic Rio Grande Rift (omitted for clarity), and the northern SE Arizona (SEAZ) ore district. F-L SZ refers to the Farewell Mt.–Lester Mt. Suture Zone. (B) The relationship between the Cordilleran foreland thrust belt and the Clementine prospect, after Hildenbrand and others (2000), and Brimhall (2017). (C) Clustering of ore deposits around the Butte district.

where "releasing steps" at ramp tops served as initial points of emplacement, subsequent pluton growth, and exceptional levels of chemical differentiation within underlying laccoliths (Brimhall and Marsh, 2017). Besides facilitating magma ascent, these localized lower pressure zones may also provide a mechanism inducing magmatic water saturation, driving magmatic-hydrothermal mineralization, and thus explaining the ubiquitous mineralization and alteration of many of the plutons in the Butte–Pioneer Mineral Belt (Brimhall and Marsh, 2017).

Analytical Methods

A large fresh rock sample (GB13-20D) of a well-exposed actinolite-calcite-titanite orbicular zone shown on the west side of the orb cupola (figs. 1, 3) was broken into pieces as free of surficial oxidation effects as possible. The freshest of these pieces were sawn into parallel slabs 1 cm thick using a Barranca Diamond BD-10 diamond saw cooled by water-soluble synthetic cutting fluid as lubricant so as to retain most of the mineral filling contained in the intact orbs. A polished thin section blank was cut to size and sent to Wagner Petrographic, where the final 30-µm-thick polished thin section slide was prepared (fig. 4). At the Australian National University the polished thin section was cut into small millimeter-scale pieces containing titanite grains and set in epoxy mounts for Sensitive High Resolution Ion MicroProbe (SHRIMP) analysis, which is a play on words as the SHRIMP analysis instrumentation is unusually large (Froude and others, 1983; Williams, 1997). The size is necessary in order have the high sensitivity and resolution capacity to analyze individual mineral grains with many distinct in situ spots so as to acquire statistics necessary to offer an accurate radiometric U/Pb age date and where possible explore the range of common lead isotopes as well.

Typically titanite ($CaTiSiO_5$) is known as a common accessory mineral in felsic granitoid rocks. However, thin section petrography of the orbicular alteration at Clementine revealed that titanite appeared to be a mineral phase formed by hydrothermal alteration, not igneous processes. As such, titanite, which contains U^{4+} substituting for Ti^{4+}, affords an opportunity to ascertain the radiometric age of titanite and hence the age of hydrothermal formation of the orb cupola. We can also infer the likely age of the associated chalcopyrite and perhaps much of the hydrothermal and magmatic processes inside of the cupola, including veins, breccias, and felsic plutons to a first approximation.

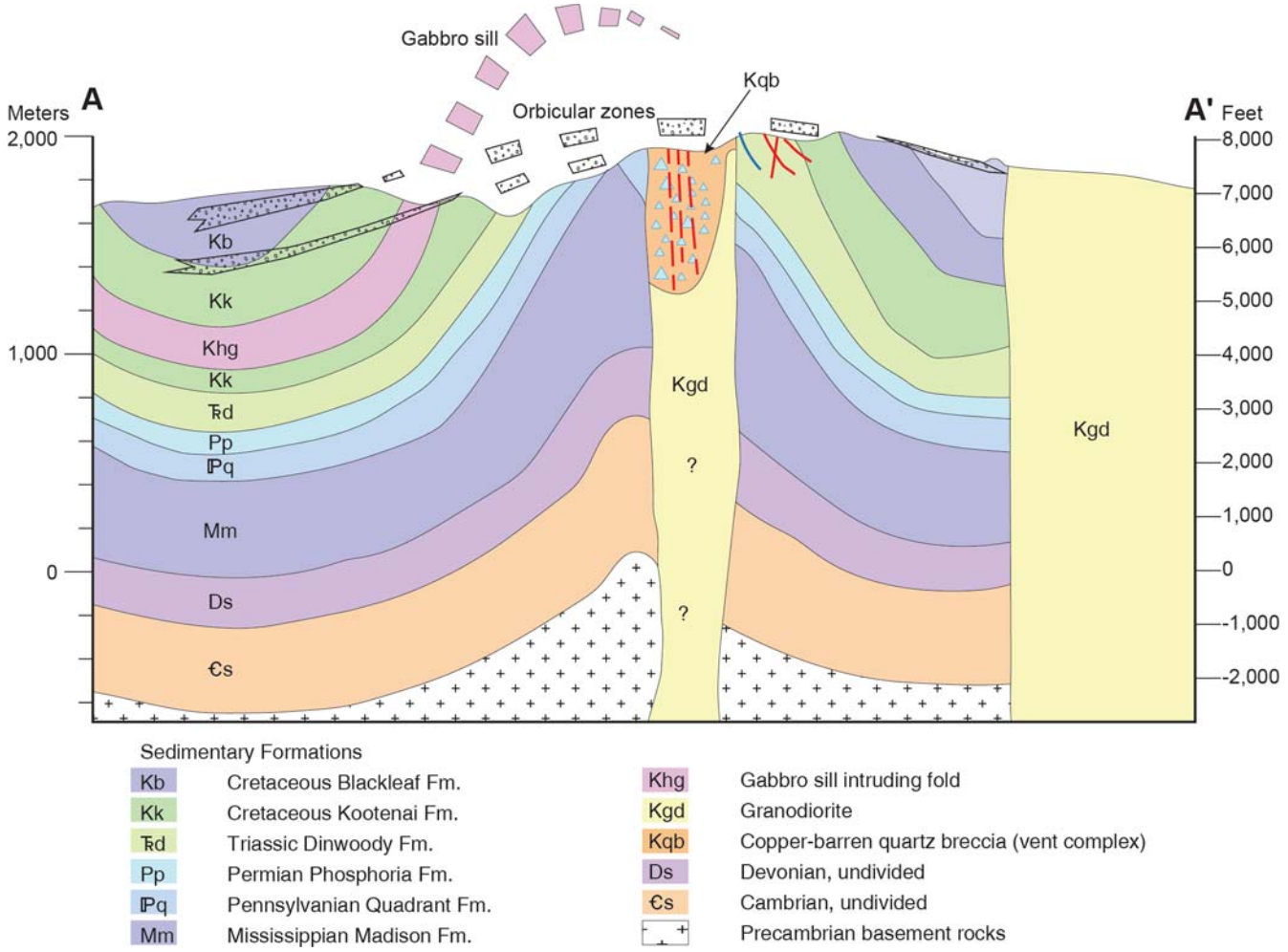

Figure 3. Interpretive vertical geological cross section of Clementine based entirely upon: (1) surface digital geological mapping and (2) approximate formation thickness. Notice the gentle outward dips of the orbicular zones and their upward closure near the present surface. The apparent dips shown here are based on the "V" patterns where mapped orbs cross steep canyons. Also, notice that the copper-barren breccia, with quartzite fragments occurring along the axial plane of the anticline, plots in the vertical vicinity of the orbicular zone projection. We interpret this to mean that fragmentation of the Quadrant Formation was related to formation of the steeply dipping, tabular copper-barren breccia zones. The location of the orbicular alteration sampled for analysis in this study is shown as Sample GB13-20D.

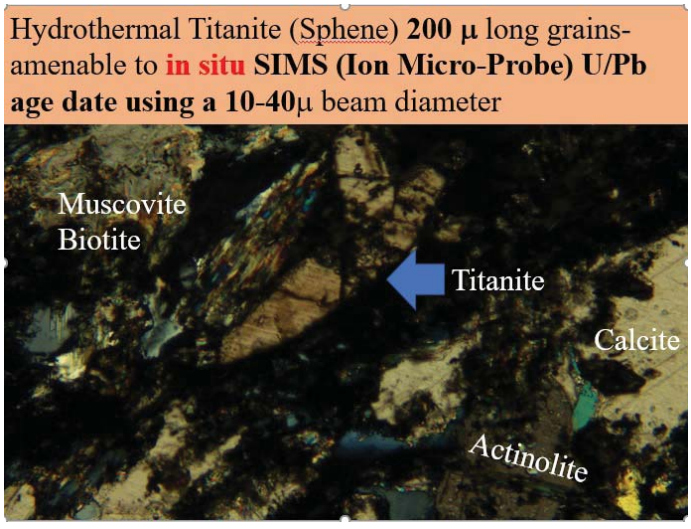

Figure 4. Photomicrograph in crossed polarizers of sample GB13-20D actinolite-calcite-titanite (sphene), biotite, muscovite, and quartz. All minerals identified optically have been verified using a Zeiss EVO-10 Variable Vacuum SEM using both secondary electron and backscattered electron imaging and qualitative chemical analyses using an energy-dispersive EDAX system.

Table 1. Summary of SHRIMP U-Pb results for Titanite from sample GB13-20D.

Area. spot	U (ppm)	Th (ppm)	Th/U	$^{206}Pb^*$ (ppm)	$^{204}Pb/^{206}Pb$	±	f_{206} %	Total $^{238}U/^{206}Pb$	±	Total $^{207}Pb/^{206}Pb$	±	Radiogenic $^{206}Pb/^{238}U$	±	Age (Ma) $^{206}Pb/^{238}U$	±
1.1	98	7.3	0.07	7.2	0.048228	0.001030	85.7	11.691	0.298	0.7309	0.0202	0.01220	0.00260	78.1	16.5
1.2	35	2.7	0.08	8.8	0.053168	0.001455	91.9	3.395	0.159	0.7928	0.0131	0.02394	0.00705	152.5	44.4
1.3	104	6.2	0.06	1.7	0.018417	0.001770	40.1	53.720	0.904	0.3658	0.0190	0.01114	0.00050	71.4	3.2
1.4	12	0.4	0.03	3.9	0.052841	0.001730	94.7	2.700	0.110	0.8177	0.0169	0.01946	0.01013	124.3	64.0
5.1	55	144.9	2.65	3.3	0.044431	0.002132	79.2	14.398	0.296	0.6792	0.0094	0.01442	0.00136	92.3	8.6
6.1	79	2.9	0.04	1.2	0.026294	0.002026	40.13	55.404	0.993	0.3657	0.0062	0.01081	0.00028	69.3	1.8
7.1	52	5.5	0.11	0.9	0.025643	0.002238	45.0	49.222	0.999	0.4040	0.0092	0.01118	0.00037	71.7	2.4
7.2	82	9.2	0.11	1.5	0.028674	0.003383	44.1	47.186	2.203	0.3978	0.0042	0.01184	0.00059	75.9	3.8
7.3	45	3.5	0.08	1.1	0.031268	0.002215	60.1	36.104	0.765	0.5245	0.0111	0.01105	0.00055	70.8	3.5
7.4	50	1.7	0.03	1.3	0.032822	0.005110	68.5	32.791	2.731	0.5909	0.0438	0.00960	0.00191	61.6	12.2
8a.1	41	8.6	0.21	1.5	0.040849	0.002171	75.29	24.048	0.731	0.6453	0.0199	0.01027	0.00124	65.9	7.9
8.1	56	9.5	0.17	1.0	0.029106	0.003717	48.3	48.759	1.063	0.4307	0.0139	0.01060	0.00047	68.0	3.0
8.2	35	8.2	0.24	2.0	0.047472	0.002174	80.8	15.045	0.632	0.6913	0.0068	0.01273	0.00128	81.6	8.2
8.3	47	7.5	0.16	1.9	0.039721	0.002047	77.2	21.294	0.437	0.6612	0.0091	0.01069	0.00090	68.5	5.7
8.4	56	9.9	0.18	2.2	0.041668	0.002292	73.97	21.548	0.415	0.6356	0.0101	0.01208	0.00091	77.4	5.8
8.5	42	7.5	0.18	1.8	0.043405	0.002561	76.8	20.319	0.459	0.6584	0.0145	0.01139	0.00118	73.0	7.5
8.6	79	13.2	0.17	2.8	0.039025	0.001437	72.7	24.391	0.444	0.6252	0.0123	0.01118	0.00087	71.7	5.6
8.7	74	13.9	0.19	1.3	0.027578	0.001892	48.7	47.017	0.848	0.4339	0.0134	0.01091	0.00045	69.9	2.9
9.1	64	9.4	0.15	1.1	0.021482	0.002137	45.6	49.223	0.932	0.4095	0.0202	0.01104	0.00059	70.8	3.7
10.1	181	27.6	0.15	1.9	0.004553	0.000715	10.10	80.399	1.186	0.1276	0.0032	0.01118	0.00017	71.7	1.1
10.2	111	16.5	0.15	1.3	0.008245	0.001232	17.7	74.370	1.264	0.1876	0.0063	0.01107	0.00022	71.0	1.4
11.1	112	18.7	0.17	2.1	0.027608	0.002796	50.2	45.138	0.753	0.4460	0.0288	0.01103	0.00085	70.7	5.4

Results

The SHRIMP data and related errors are summarized in table 1 for the 22 spots analyzed under the ion beam.

A central concept to using the data in table 1 is that ^{238}U decays to ^{206}Pb with a half-life of 4.468 x 10^9 years and ^{235}U decays to ^{207}Pb with a half-life of 0.707 x 10^9 years. ^{238}U is the more abundant U isotope in the earth, amounting to about 99.2745%, while ^{235}U constitutes only about 0.72%. ^{204}Pb is a stable non-radiogenic isotope of Pb that is used to normalize the ^{206}Pb and ^{207}Pb measurements as shown in equations 1 and 2 for ^{238}U decay to ^{206}Pb and ^{235}U decay to ^{207}Pb, respectively. λ^{238} and λ^{235} are the radiometric decay rate constants for ^{238}U and ^{235}U, respectively, and t is time. λ^{238} is 1.55125 x 10^{-10} and λ^{235} is 9.8485 x 10^{-10} (Steiger and Jäger, 1977).

$$\left(\frac{^{206}Pb}{^{204}Pb}\right) = \left(\frac{^{206}Pb}{^{204}Pb}\right)_0 + \left(\frac{^{238}U}{^{204}Pb}\right)\left(e^{\lambda_{238}t} - 1\right) \qquad 1$$

$$\left(\frac{^{207}Pb}{^{204}Pb}\right) = \left(\frac{^{207}Pb}{^{204}Pb}\right)_0 + \left(\frac{^{235}U}{^{204}Pb}\right)\left(e^{\lambda_{235}t} - 1\right) \qquad 2$$

Notice that both equations 1 and 2 are of the form $y = a_0 + X_m$, where a_0 is the y-intercept where x equals zero, x is $^{238}U/^{204}Pb$ (equation 1) or $^{235}U/^{204}Pb$ (equation 2), and the terms with ($e^{\lambda 238t}$–1) or ($e^{\lambda 235t}$–1) are the slope, *m*. The y-intercept values $(^{206}Pb/^{204}Pb)_0$ and $(^{207}Pb/^{204}Pb)_0$ are called initial Pb or common lead in contrast to radiogenic Pb formed by U decay after the titanite formed, which is the fraction used in radiometric dating. Common Pb can pose a serious challenge to accurate radiometric dating so minerals like zircon are usually sought out as their structure precludes inclusion of much Pb while having a very high U/Pb ratio. Titanite may have substantial common or initial Pb so that special care must be taken to acquire an accurate radiometric age. The initial Pb ratio can be determined by making Isochron plots as commonly done in Rb/Sr dating. Here

instead, the **ratio** of the common initial Pb values was determined by using a method derived and described by Tera and Wasserburg (1972), working with lunar samples and making no assumption about the magnitude of initial or common lead ratios, that is the y-intercepts in equations 1 and 2. Instead, measured **total** $^{207}Pb/^{206}Pb$ ratios are plotted against $^{238}U/^{206}Pb$ ratios. Ratios are not corrected for initial or common Pb. A series of *in situ* sample spots with different U/Pb values containing common Pb will plot along a straight line that intercepts the closed system 'concordia' curve at a point where $^{207}Pb/^{206}Pb$ and $^{238}U/^{206}Pb$ ages are equal. The intercept of the regression line is the initial $^{207}Pb/^{206}Pb$ because a sample with a $^{238}U/^{206}Pb$ ratio of 0 will retain its initial Pb isotopic composition. In simple cases multiple analyses define a discordia line whose intersections with the Concordia curve indicates both the time of formation of the titanite and the composition of the common lead. The Tera–Wasserburg coordinate system has now been tested for almost 50 years on a wide variety of complex sample types with detailed assessment of errors (Lugwig, 1998). The Tera–Wasserburg plot can be expanded into a three-dimensional plot where the third axis is defined by $^{204}Pb/^{206}Pb$. This 3-D plot allows dealing with samples comprising substantial amounts of common Pb without requiring *a priori* correction. The data, uncorrected for common Pb, are generally visualized as projections on the $^{207}Pb/^{206}Pb$ and $^{238}U/^{206}Pb$ plane, and for concordant populations having different proportions of radiogenic to common Pb they define a line whose intersection with Concordia yields the age of crystallization. A version of the plot reduced to 2-D is used occasionally to visualize and interpret high common Pb data without measuring $^{204}Pb/^{206}Pb$.

In figure 5A, a Tera–Wasserburg plot for the 22 titanite SHRIMP analysis spots in Sample GB13-20D is shown in relation to the Concordia closed system curve in black with age ticks. Notice that the data shown with their error ellipses define a linear relationship from the upper left intercept with Concordia showing the

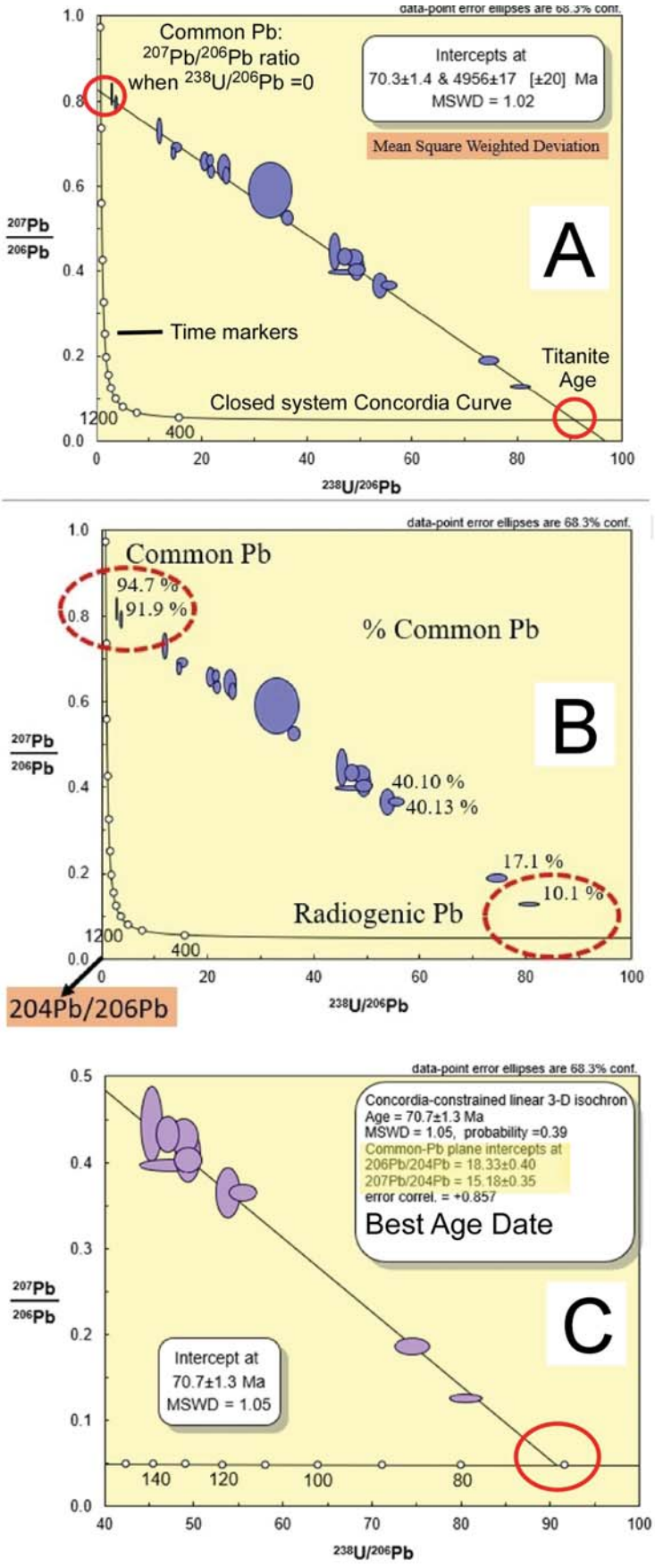

Figure 5. (A) Tera–Wasserburg plots of discordant U/Pb data on titanite (sphene) in sample GB13-20D actinolite-calcite-titanite orbicules shown in figures 1A and 3. The linear discordia line intersects the Wetherill concordia curve in two places: the lower right intersection gives the radiometric age of the hydrothermal titanite. The upper left intercepts provide the common Pb composition. (B) The percent common lead in each SHRIMP analysis spot, from 94.7% in the upper left down to 10.1% in the lower right, which is mostly radiogenic Pb formed *in situ* after the titanite crystallized from the ore-forming hydrothermal solution and became a closed isotopic system. Notice that the $^{207}Pb/^{206}Pb$ ratio of the common lead is about 0.80 on the Y-axis. (C) The best age of 70.7 Ma, where the discordia line intersects the concordia curve and almost all the Pb is radiogenic. In addition to the radiometric age determination, the common Pb plane intercepts yield a $^{207}Pb/^{206}Pb$ ratio 0.8282 on the Y-axis by regression.

common Pb ratio $^{207}Pb/^{206}Pb$ near a value of 0.8 down to lower right where the radiometric age of 70.3 million years (Ma) is shown. In figure 5B the percent common lead in each SHRIMP analysis spot is shown varying from 94.7% in the upper left down to 10.1% in the lower right, which is mostly radiogenic Pb formed in situ after the titanite crystalized from the ore-forming hydrothermal solution and became a closed isotopic system. Notice that the y-intercept $^{207}Pb/^{206}Pb$ ratio of the common lead is about 0.80 on the y-axis. Figure 5C shows the best regressed age of the titanite 70.7 Ma where the Discordia line intersects the Concordia curve and almost all the Pb is radiogenic. In addition, two fundamental Pb isotope ratios central to our work are show in figure 5C: regressions in the common Pb plane yield intercepts with the $^{206}Pb/^{204}Pb$ ratio at 18.33 with an error of 0.40 and a $^{207}Pb/^{204}Pb$ ratio of 15.18 with an error of 0.35. The ratio of $^{207}Pb/^{204}Pb$ and $^{206}Pb/^{204}Pb$, which is 15.18/18.33, is 0.8282.

Comparison of SHRIMP Age of Clementine with Plutons and Ore Deposit Ages Nearby

In figure 6, the radiometric age of Clementine (70.7 Ma) is shown in relation to ages of ore deposits in the surrounding area. Clementine, with its U/Pb age of 70.7 Ma, occurs within the general outline of the Boulder Batholith and as such is clearly north of the Pioneer Batholith. Zen (1996a), based on Rb/Sr isotopic difference, asserted that the boundary between the two batholiths was the Sawmill Gulch Fault south of the Big Hole River Canyon pluton. The Butte pre-Mainstage is shown as 68–66 Ma, with the Mainstage as 62.5 Ma (Houston and Dilles, 2013). Dates on the Big Hole Canyon pluton immediately south of Clementine are shown as 75.4 to 74.7 Ma for the inclusion-bearing granodiorite biotite (Zinter and others, 1983), although these dates are younger than the earlier, more mafic phases. Dates on rocks south of the Sawmill Canyon Fault, including Cannivan Gulch, are shown as 68 to 66.8 Ma (Schmidt and others, 1979). Fresh pluton ages reported by Zen (1988) are shown as 72 Ma for the Uphill Creek granodiorite, 74.8 Ma for the Stine Creek pluton, and 64 Ma for the leucogranite of Bobs Lake. The Pioneer Batholith has multiple groupings of ages (Snee and others, 1983): Group 1 (83–80 Ma), 2 (79–76 Ma), 3 (76.5–74.5 Ma), 4 (74.5–72.0 Ma), 5 (72–69.5 Ma), 6 (72–69.5 Ma), and 7 (67–66

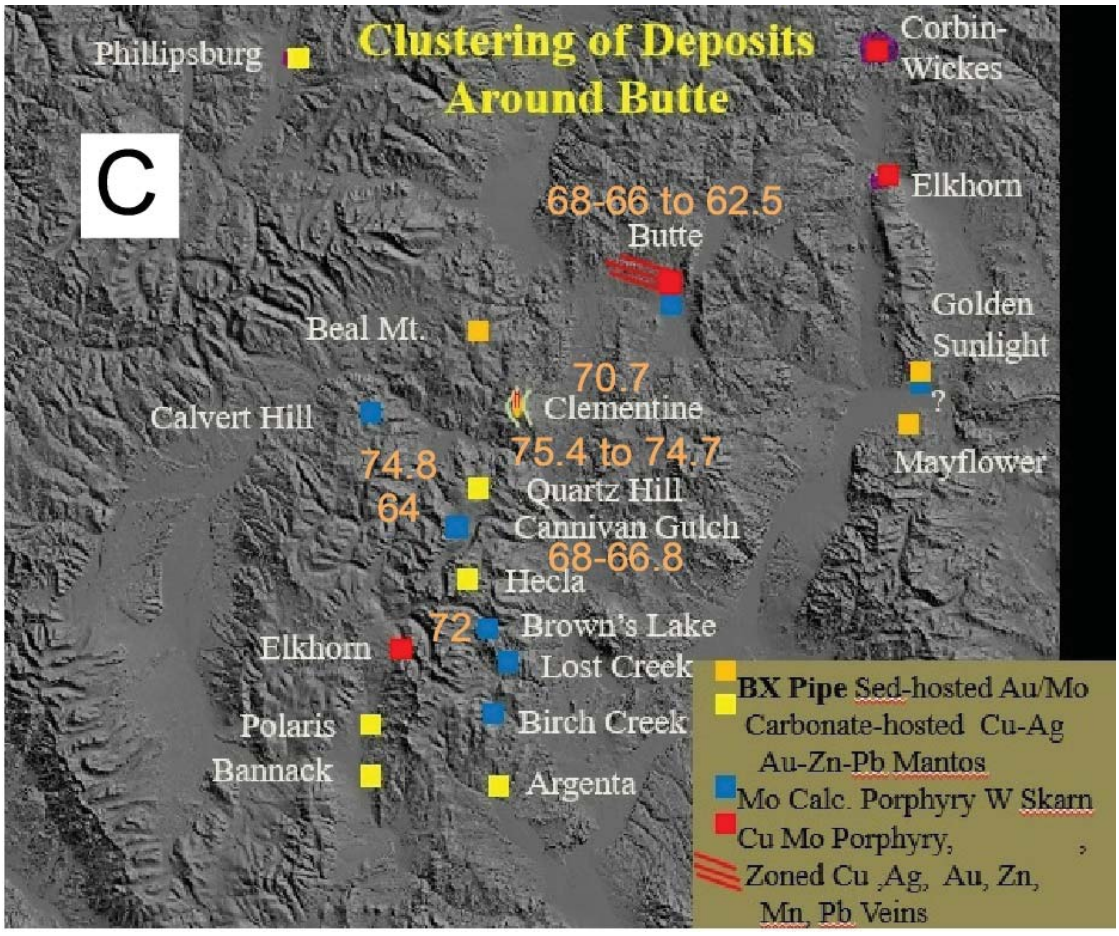

Figure 6. Radiometric (K-Ar, $^{40}Ar/^{39}Ar$ dates of plutons and mineralization.

Ma). Snee and others (1983) notes that these age ranges are $^{40}Ar/^{39}Ar$ cooling stages and not necessarily pluton crystallization ages.

Zen (1996a,b) asserts that the initial Sr (iSr) values of the Pioneer Batholith stand in contrast to those of the Boulder Batholith situated to the north–northeast. Among the highest iSr ratios measured are porphyry dikes near Hecla (Zen, 1996b). Rocks of the two batholiths are petrographically and chemically similar; they have the same age range and share comparable tectonic setting and history. However, the Boulder Batholith (both the "Main Series" and the "Sodic Series" of Tilling, 1973) has much lower values of iSr (Doe and others, 1968), ranging from 0.7055 to 0.7092; an isopleth of 0.710 fully separates the two batholiths, and this boundary is in fact mappable, at the current level of erosion, as the north–northwest-striking Sawmill

Gulch–Trusty Gulch fault system (fig. 1; Zen, 1988; Arth and others, 1986). Comparing the Clementine SHRIMP titanite age of 70.7 Ma with the variety of ages shown in figure 6 shows that the hydrothermal processes by which the orbicular alteration formed and the titanite precipitated from high-temperature aqueous solutions are clearly well within the age ranges of the plutons and alteration ages of large and minor ore deposits.

Titanite Stability in Relation to Potassic Alteration and Carbon Dioxide Content of the Fluid

Given the importance of potassic alteration associated with high-temperature mineralization in porphyry copper genesis and in textures observed at Clementine (fig. 1A) where a white bleached zone surrounds actinolite-filled orbs with titanite and calcite (fig. 1C), thermodynamic phase equilibria help explain the textures (fig. 7). While the most abundant mineral within orbicular alteration is actinolite, the titanite, calcite, pyrrhotite, chalcopyrite, ilmenite, quartz, and the annite component in biotite ($KFe_3AlSi_3O_{10}(OH)_2$) are more accurately represented in phase diagrams, given the broad solid solution range of actinolite, which is a complex amphibole with wide solid solution ranges and hence complex and largely unknown thermodynamic values. A new equilibrium phase diagram show in figure 7 was calculated here using computer program SUPCRIT, which was developed at U.C. Berkeley by H.C. Helgeson and students (Johnson and others, 1992) and revised by Zimmer and others (2016) with improvements in the thermodynamic data, specifically the addition of ilmenite (Holland and Powell, 2011), which is critical for this study and lacking in the earlier data set. The version of SUPCRITBL (for Bloomington, Indiana) used here can be accessed at: https://www.indiana.edu/~hydrogeo/supcrtbl.html.

One of the phase boundaries, shown as a heavy red line 1 in figure 7, is equation 3:

$$\text{Titanite} + \text{Pyrrhotite} + CO_2 + \tfrac{1}{2} O_2 = \text{Ilmenite} + \text{Calcite} + \text{Quartz} + \tfrac{1}{2} S_2 \qquad (3)$$

In reaction 3, the stoichiometric coefficients are written so as to conserve moles of elements in solid phases and use only O2, S2, and CO_2 to balance the total moles of the solid phases. Using this convention (Holland, 1959) and composing the equilibrium constant, then taking its log yields equation 4, which is the algebraic equation for the heavy red line 1:

$$\log fS_2 = 2\log K + \log fO_2 + 2\log fCO_2 \qquad (4)$$

Biotite-bearing hornfels wall rock formed as the earliest manifestation of alteration in the regions near the orbs at the diffusive/advective boundary. Many orbs studied in thin section have a microscopic biotite crackle veinlet that appears to have been the feeder channel for the orbs. With the start of orb growth, the fluids reaching the area probably were in equilibrium with biotite (annite) with a fugacity of CO_2 such that biotite was stable inside the orbs as well. However, figure 7 shows that titanite–ilmenite boundaries are sensitive to CO_2 fugacity and move accordingly, and under specific conditions may migrate outside the biotite stability field. What process caused the selective destruction of fine-grained biotite in the white ring surrounding the actinolite-titanite-calcite-quartz orb apparently involved elevating the fugacity of CO_2 slightly outside the biotite stability

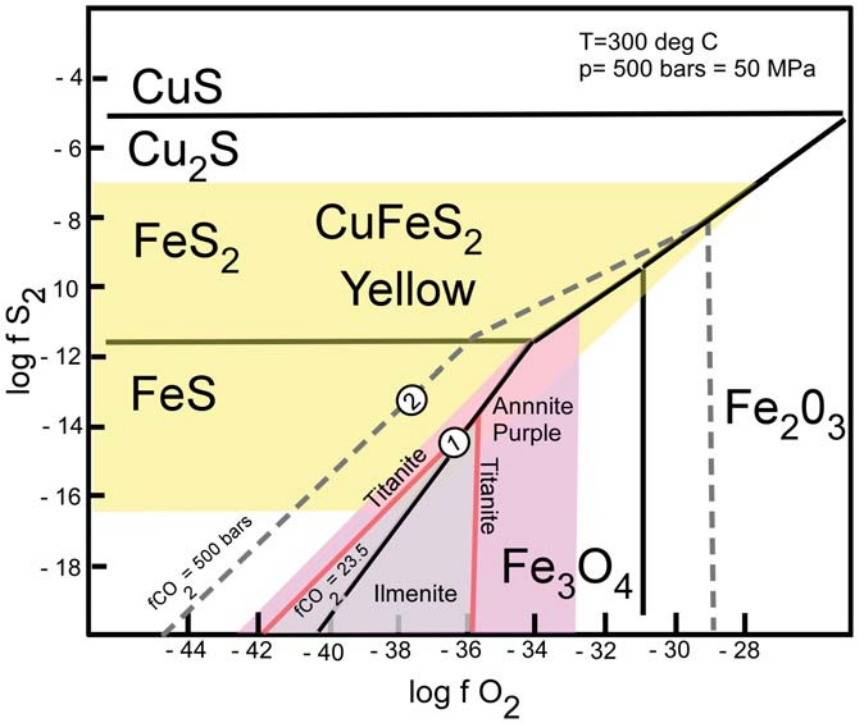

Figure 7. The heavy solid lines define the stability fields of pyrrhotite (FeS), pyrite (FeS_2), magnetite (Fe_3O_4), hematite (Fe_2O_3), covellite (CuS), and chalcocite (Cu_2S; Holland, 1959, 1965; Meyer and Hemley, 1967). The chalcopyrite field is shown in yellow surrounded by bornite (Cu_5FeS_4; Brimhall, 1980). The annite component of biotite yields outwards to orthoclase in purple (Brimhall, 1980), where all the mineral–solution–gas equilibrium are presented for this phase diagram. Here, ilmenite in gray is added surrounded by titanite shown in purple. The mineral assemblage in rock sample GB13-20D consisting of titanite, pyrrhotite, chalcopyrite, ilmenite, calcite, quartz with biotite (annite, heavy red line 1) represents the main orbicule mineralogy. A small partial pressure of CO_2 gas of 23.5 bars (out of 500 bars total pressure) is necessary for titanite and ilmenite to have equilibrated with both pyrrhotite and chalcopyrite. At lower CO_2 pressure less than 23.5 bars the titanite–ilmenite boundary would not be at equilibrium with chalcopyrite at the conditions shown of 300°C and 500 bars (50 Mpa). As the CO_2 pressure increases, the ilmenite stability field expands at the expense of titanite until at the fugacity of CO_2 equal to the total pressure of 500 bars (heavy dashed gray line 2), titanite and ilmenite are stable well outside the biotite (annite) field. We interpret the white rings surrounding the orbs shown in figure 1C as having formed with slightly elevated CO_2 pressures above about 30 bars so that biotite in the surrounding hornfels was destroyed.

field, perhaps about 30 bars (outside the purple area in fig. 5). It is fairly clear that fluid migration through the thick, highly reactive calcium carbonate-rich rock formations at depth in the axial plane of the anticline (fig. 3), where the Madison Limestone has a stratigraphic thickness of about 500 m, played an important role as a chemical buffer capable of supplying CO_2 gas. During orb growth, the fugacity of CO_2 was at least 23.5 bar to stabilize chalcopyrite. However, the CO_2 fugacity apparently rose even higher to a value above 30 bars, which caused the titanite–ilmenite line to move upwards and outside the biotite (annite) stability field. The white bleached color is due to local biotite destruction within the ring annulus. The hydrothermal fluid was either in equilibrium or slightly out of equilibrium with biotite, which is an essential alteration assemblage in early porphyry copper deposit genesis.

Discussion

On a district scale, the axially symmetric position of the distal orbicular actinolite-titanite-calcite alteration with respect to the vein gossans, breccias, and felsic plutons is highly suggestive that all these features are genetically related. In cross section, the orbicular alteration appears to dip away from the center of the zoning pattern, implying that it is both distal and uppermost and was emplaced with clear regional structural control near the axial crest of a doubly plunging anticline confined by the overlying Grasshopper thrust plate. The entire system was emplaced between Archean crustal blocks, which are delimited by Proterozoic accretionary tectonic zones interpreted as sutures representing early Proterozoic subduction zones where oceans disappeared. Major ore deposits sharing this crustal heritage include Butte, Bingham, Henderson, and Questa. On a smaller scale, the clustering of ore deposits around the Butte district shows that Clementine occurs within a north–south-striking belt of old mining districts (Quartz Hill, Cannivan Gulch, Helcla). all of which occur along the crest of a regional anticlinorium. Furthermore, each district occurs at doubling-plunging anticlines or domes. By radiometrically dating the titanite contained within the actonolite orbs, we showed that the age of 70.7 Ma fits well within the magmatic history of the Boulder Batholith, and the mineralization in the Butte District. The deposits to the south of Clementine (Quartz Hill, Cannivan Gulch, and Hecla) formed within a batholith that is isoptically distinct and clearly more crustally derived. What the Clementine system did share with the other deposits was the frontal thrust plane of the Sevier Fold and Thrust Belt. Regardless of the mantle or crustal source region, the magmas in both the Boulder and Pioneer Batholiths appear to have intruded up the same regional thrust fault ramps. Laccolith bodies at depth seem to be where most of the chemical fractionation occurs that is required for the high levels of metal enrichment to form the ore deposits.

Conclusions

The intent of this work on orbicular alteration is to revise the distal and upper reaches of the geo-spatial patterns of porphyry copper paradigm and provide new field methods that help support the transition to deep porphyry copper exploration. Orb mapping can assist in targeting large deep porphyry copper deposits during early exploration through properly interpreting the orbicular zonation surrounding the typical alteration halo around these large intrusive systems as the exterior of the system's fracture pattern, providing a bullseye to focus follow-up exploration.

Orb alteration makes this subtle physical boundary feature macroscopically visible and contributes a powerful new mapping tool in lithologies where orbs are likely to form, such as in sedimentary and other wall rocks with connected pore space, allowing intergranular diffusion rather than in non-porous rocks with interlocking grains. The utility of orb cupolas as a targeting tool in deep exploration stems from several observations. First, it has been demonstrated that actinolite-titanite-calcite orbs can be mapped successfully even in completely timbered terrain and related geo-spatially to more proximal zone vein gossan systems, breccia bodies, and plutons as the distal and superjacent hydrothermal alteration feature. Second, the orbicular zones mark the position of a key hydrodynamic boundary that is largely invisible otherwise, which is the peripheral edge of the mineralized fracture permeability network at the time of coupled wall rock alteration and mineralization because disseminated chalcopyrite occurs near the orbs. Third, it has been demonstrated here that accurate radiometric dating of titanite (sphene) occurring within the actinolite-calcite-filled orbs is possible. Moreover, radiometric SHRIMP U/Pb dating works effectively even when high levels of common Pb occur within the hydrothermal titanite as long as the Terra–Wasserburg (1972) method is used, since it requires no assumptions about common lead compositions to generate a reliable radiometric age date. Fourth, if during geological mapping early on in exploration of a new region, orbs are found and the titanite ages ascertained, the resultant radiometric age can be a decisive factor in readily establishing the age of likely copper mineralization and compared with other age dates on plutons and regional plutonic episodes of metallogenic interest. Fifth, Concordia-constrained 3-D isochrons in fact yield both accurate ages and accurate common lead plane intercepts of $^{206}Pb/^{204}Pb$ and $^{207}Pb/^{204}Pb$ ratios. These common lead ratios have utility in comparing data on a new deposit with known common Pb ratios in productive mineral belts (Zartman, 1974) that will be described in a future publication. Sixth, since it has now been shown at the Clementine prospect that springs today occur near the orb bands, it is inferred that the gross permeability of the hornfels-altered rocks inside the orb cupola is lower than those outside the cupola in unaltered formations, forcing groundwater upwards into springs. Hence, the spatial association of springs with orb bands provide another exploration tool of using mapped springs from U.S. Geological Survey topographic maps to: (1) help find and map orbicular alteration and associated disseminated sulfide mineralization in new districts, and (2) infer on a potential district scale the position, size, and orientation of a new prospective region of interest once the orb pattern has been mapped.

More broadly, the fundamental challenge in advancing the paradigm used in deep porphyry copper deposit exploration is assembling a practical, cost-effective, new strategy based on definitive pathfinder mineral-isotopic indicators that significantly enlarges the target size, and provides regional results that can be classified so that only the largest deposits stand out in relation to the subordinate deposits during early stage, pre-drilling exploration. Hence, the essence of the approach described here is that for deep deposit exploration to prove more effective than it has in the past decade, PCD pathfinder mineral-isotopic indicators may offer a more effective strategy than the present search for traditional features of copper deposits exposed at their mid-sections, including leached cappings above supergene enrichment blankets, rather than the upper, low sulfide content, reaches of deep deposits amenable to deep underground mining with a far smaller environmental footprint.

It is suggested here that for deep PCD mineral exploration to once again become successful, a transformation in how applied science is judged in joint venture decisions is required as a "more of the same" approach has not worked. First, exploring through the tops of prospective new deep porphyry copper deposits means confronting the realities of a largely unfamiliar geological domain above the current upper tops of the porphyry copper paradigms, based on mined ore deposits whose surface exposures intersected the surface within or somewhat above ore grade levels, not 500 to 1,000 m above ore grade level as in deep deposits. Hence, special care

should be taken in evaluating deep prospect geology. A small shallow district with strong epithermal indications and a multitude of conventional data such as soil sample arrays and Cu assays might appear more prospective than a new superjacent zone defined by a large radiometrically dated orb ring surrounding a vein system and possible parental pluton but with fewer assay data. Risk aversion prompted by confirmation bias could motivate selecting the former as a superior target, especially if 3-D virtual reality viewing of prospect data density is deemed to be a decisive factor. In contrast, a radiometric titanite age that makes geological sense with respect to regional metallogenic magmatic and hydrothermal events, the size of the orb ring, and common Pb ratios may offer a more discerning glimpse of what could occur at depth than a myriad of assay data alone. Similarly, given the need to advance understanding of the superjacent zone in terms of new features, work on prospects needs to include support for geological mapping, polished thin section petrography, and petrology. New features observed may appear odd at first, but only when such observations are respected and mapped, and not merely discounted and deemed outside the realm of the PCD model, will new useful features be documented and put into widespread use. It is hoped that this work will help spur organizations to allocate personnel and resources to undertake advanced scientific mapping to find and describe new features of the deep PCD superjacent zone. Finally, for fieldwork to be effective, ergonomics must be considered with vehicles used to advantage supporting geologists with drop off and pick up shuttles to save time and energy.

Acknowledgments

Doug Fuerstenau reviewed an early version of this manuscript, helping to improve its clarity significantly. Colleen Elliott and Stanley Korzeb also provided reviews. For the first author, this study is a coalescence of methods learned over a lifetime and inspired early on by a few special teachers. As an undergraduate at U.C. Berkeley (1965–1969), Brimhall is grateful for the exceptional opportunity of having learned the use of the petrographic microscope from two masters of optical mineralogy who were visiting professors: K. Naha of the Indian Institute of Technology Kharagpur, who urged us to: “learn rock-forming and accessory minerals like your friends—by sight,” and Stewart Agrell of Cambridge University, whose igneous petrology course included descriptions of orbicular rocks of igneous origin, which allowed Brimhall to understand how distinct, in contrast, are the hydrothermal processes that formed the actinolite-calcite-titanite orbs at Clementine. Two sabbatical leaves also afforded special opportunities to explore basic U/Pb isotopic principles implemented here. At Cal Tech (1985–1986), Brimhall absorbed U/Pb isotopic material from Clair Patterson and Geri Wasserburg, and at the Australian National University in Canberra (1992–1993), he learned SHRIMP analysis from Bill Compston, Ian Williams, and Trevor Ireland (Brimhall and others, 1994). In recent years his knowledge of indicator mineralogy in diamond exploration benefited from close associations with Ray Morley and Hugo Dummett (formerly of BHP San Francisco Global Exploration). Mary Jane Brimhall has served as the principal field safety coordinator, monitoring the locations of all personnel using SPOT satellite uplinkers during all the fieldwork involved in our geological mapping spanning 7 years. Ed Rogers has been a steadfast field companion in challenging terrains for a decade. Jay Ague was instrumental in locating an up-to-date thermodynamic code to calculate phase equilibria. Abel Vanegas provided technical support in digital mapping and community outreach education. Ray Morley, Dan Kunz, and Doug Fuerstenau are thanked for their ongoing enthusiastic commentary and support. Chris Gammons and Colleen Elliott of Montana Tech and the Montana Bureau of Mines and Geology continue to provide insightful scientific dialogue and access to laboratory equipment. Jim Freestone has conducted all forest restoration activities to the satisfaction of the USFS and Montana DEQ for Clementine Exploration. Jim and John Lundborg have also been a major help in shuttling field crews and vehicles, making mapping and sampling possible in steep forested terrain. Tim Teague provided the SEM and EDAX. Erik Torgeson (U.S. Forest Service) is thanked for field site visits of USFS staff so that we can maintain good working relations with the U.S. Forest Service.

References

Arth, J., Zen, E-An, Sellers, G., and Hammarstrom, J., 1986, High initial Sr isotopic ratios and evidence for magma mixing in the Pioneer Batholith of southwest Montana: Journal of Geology, v. 94, p. 419–430.

Atkinson, W., and Einaudi, M.T., 1978, Skarn formation and mineralization in the contact aureole at Carr Fork, Bingham, Utah: Economic Geology, v. 75, p. 1326–1365.

Brimhall, G.H., 1980, Deep hypogene oxidation of porphyry copper potassium-silicate protores: A theoretical evaluation of the copper remobilization hypothesis: Economic Geology, v. 75, p. 384–409.

Brimhall, G.H., Compston, W., Williams, I.S., Reinfrank, R.F., and Lewis, C.J., 1994, Darwinian zircons as provenance tracers of dust-size exotic components in laterites: Mass balance and SHRIMP ion microprobe results, in Soil micromorphology: Studies in management and genesis, Ringrose-Voase, A.J., and Humphreys, G.S., eds.: Amsterdam, Elsevier, p. 65–82.

Brimhall, G.H., and Marsh, B.D., 2017, Nature of the mineralization and alteration at the Clementine porphyry copper prospect in the northern Pioneer Mountains of southwest Montana: Montana Bureau of Mines and Geology Open-File Report 699, p. 55–58.

Brimhall, G., 2018, Orbicular alteration at the Clementine porphyry copper prospect of southwest Montana: Defining the edges of advective flow in the porphyry copper paradigm: Montana Bureau of Mines and Geology Special Publication 120, p. 71–83.

Doe, B., Tilling, R., Hedge, C., and Klepper, 1968, Lead and strontium isotope studies of the Boulder Batholith, southwestern Montana: Economic Geology, v. 63, p. 884–906.

Foster, D., Mueller, P., Mogk, D., Wooden, J., and Vogl, J., 2006, Proterozoic evolution of the western margin of the Wyoming craton: Implications for the tectonic and magmatic evolution of the northern Rocky Mountains: Canadian Journal of Earth Science, v. 43, p. 1601–1619.

Froude, D., Ireland, T., Kinny, P., Williams, I., Compston, W., Williams, I., and Myers, J., 1983, Ion microprobe identification of 4,100-4,200 Myr-old terrestrial zircons, Nature, v. 304 p. 616–618.

Gustafson, L., and Hunt, J.P., 1975, The porphyry copper deposit at El Salvador, Chile: Economic Geology, v. 70, p. 857–912.

Hildenbrand, T.G., Berger, B.R., Jachens, R.C., and Ludington, S.D., 2000, Regional crustal structures and their relationship to the distribution of ore deposits in the Western United States, based on magnetic and gravity: Economic Geology, v. 95, p. 1583–1603.

Holland, R., 1959, Stability relations among the oxides, sulfides, sulfates and carbonates of ore and gangue metals, [Part] 1 of Some applications of thermochemical data to problems of ore deposits: Economic Geology, v. 54, p. 184–233.

Holland, R., 1965, Some applications of thermochemical data to problems of ore deposits; [Part] 2, Mineral assemblages and the composition of ore forming fluids: Economic Geology, v. 60, p. 1101–1166.

Holland, T., and Powell, R., 2011, An improved and extended internally consistent thermodynamic dataset for phases of petrological interest, involving a new equation of state for solids: Journal of Metamorphic Petrology v. 29, no. 3, p. 333–303.

Houston, R., and Dilles, J., 2013, Structural geologic evolution of the Butte district, Montana: Economic Geology, v. 108, p. 1397–1424.

John, D.A., Ayuso, R.A., Barton, M.D., Blakely, R.J., Bodnar, R.J., Dilles, J.H., Gray, F., Graybeal, F.T., Mars, J.C., McPhee, D.K., Seal, R.R., Taylor, R.D., and Vikre, P.G., 2010, Porphyry copper deposit model, Chap. B of Mineral deposit models for resource assessment: U.S. Geological Survey Scientific Investigations Report 2010–5070–B, 169 p.

Johnson, J.W., Oelkers, E.H., and Helgeson, H.C. (1992) SUPCRT92—A software package for calculating the standard molal thermodynamic properties of minerals, gases, aqueous species, and reactions from 1-bar to 5000-bar and 0°C to 1000°C: Computer and Geosciences, v. 18, p. 899–947.

Kalakay, T., John, B.E., and Lageson, D.R., 2001, Fault-controlled pluton emplacement in the Sevier fold-and-thrust belt of southwest Montana, USA: Journal of Structural Geology, v. 23, p. 1151–1165.

Karlstrom, K.E.,Whitmeyer, S.J., Dueker, K.,Wiliams, M.L., Bowring, S.A., Levander, A., Humphreys, E.D., and Keller, G.R., the CD-ROM Working Group, 2004, Synthesis of results from the CD-ROM experiment: 4-D image of the lithosphere beneath the Rocky Mountains and implications for understanding the evolution of continental lithosphere, in Karlstrom, K.E., and Keller, G.R., eds., The Rocky Mountain region: An evolving lithosphere —Tectonics, geochemistry, and geophysics: Geophysical Monograph Series, 154, p. 421–480.

Lowell, J.D., and Guilbert, J., 1970, Lateral and vertical alteration-mineralization zoning in porphyry ore deposits: Economic Geology, v. 65, p. 373–408.

Meyer, C., and Hemley, 1967, Wall rock alteration, in Geochemistry of hydrothermal ore deposits, Barnes, H.L., ed.: New York, Holt, Rinehart and Winston, p. 166–235.

Mueller, P., Heatherington, A., Kelly, D., Wooden, J., and Mogk, D., 2002, Paleoproterozoic crust within the Great Falls tectonic zone: Implications for the assembly of southern Laurentia: Geology, v. 30, p. 127–130.

Pettke, T., Oberli, F., and Heinrich, C., 2010, The magma and metal source of giant porphyry-type ore deposits, based on lead isotope microanalysis of individual fluid inclusion: Earth and Planetary Science Letters 296 (2010) 267–277.

Schaffer, R., 2018, Crisis in discovery; Improving the business paradigm for mineral exploration: Mining Engineering, May Issue, p. 26–27.

Schmidt, H., Worthington, J., and Thomassen, R., 1979, K-Ar dates for mineralization in the White-Cloud-Cannivan Gulch porphyry molybdenum belt of Idaho and Montana: Discussion: Economic Geology, v. 74, p. 699.

Schodde, R., 2013, Long term outlook for the global exploration industry: Geological Society of South Africa, Geo Forum Conference, Gloom or Boom?: Johannesburg, 2–5 July 2013, Oral Presentation.

Sillitoe, R.H., 2010, Porphyry copper systems: Economic Geology, v. 105, p. 3–41.

Sillitoe, R.H., Tolman, J., and van Kerkvoort, G., 2013, Geology of the Caspiche porphyry gold–copper deposit, Maricunga belt, northern Chile: Economic Geology, v. 108, p. 585–604.

Sillitoe, R.H., Burgoa, C., and Hopper, D.R., 2016, Porphyry copper discovery beneath the Valeriano lithocap, Chile: SEG Newsletter, no. 106, July 2016, p. 1, 15–20.

Snee, L., Sutter, J., and Zen, E-an, 1983, Ages of emplacement and cooling history of the Pioneer Batholith, southwest Montana: Geological Society of America Abstract, v. 15, no. 5, p. 412.

Steiger, R. H., and Jäger, E., 1977, Subcommission on geochronology: Convention on the use of decay constants in geo- and cosmochronology: Earth and Planetary Science Letters, v. 36, no. 3, p. 359–362.

Tera, F., and Wasserburg, G.J., 1972, U-Th-Pb systematics in three Apollo 14 basalts and the problem of initial Pb in lunar rocks: Earth and Planetary Science Letters, v. 14, p. 281–304.

Tilling, R., 1973, The Boulder Batholith, Montana: Product of two contemporaneous but chemically and isotopically distinct magma series: Society of Economic Geologists, Butte Field Meeting Guidebook U.S.: Butte, Montana.

Williams, I., 1997, U-Th-Pb geochronology by ion microprobe, in Society of Economic Geologists, Reviews in Economic Geology, v. 7, p. 1–36.

Wood, D., 2016, We must change exploration thinking in order to discover future orebodies: SEG Newsletter, no. 105, p. 16–18.

Wood, D., and Hedenquist, J., 2019, Mineral exploration: Discovering and defining ore deposits: SEG Newsletter, no. 116, p. 1, 11–22.

Zartman, R., 1974, Lead isotopic provinces in the cordillera of the western United States and their geologic significance: Economic Geology, v. 69, p. 792–805.

Zen, E-An, 1988, Bedrock geology of the Vipond Park quadrangle: U.S. Geological Survey, Bulletin 1625.

Zen, E-An, 1996a, Generation of magmas of the Pioneer Batholith and geologically-constrained thermal model: U.S. Geological Survey Open File Report 96-98.

Zen, E-An, 1996b, Plutons in the eastern part of the Pioneer Batholith: Field relations and petrographic descriptions: U.S. Geological Survey Open File Report 96-97.

Zinter, G., Snee, L., and Sutter, J., 1983, Geology, petrology, and age of emplacement of the Big Hole Canyon intrusion near Dewey, southwest Montana: Geological Society of America Abstract, v. 15, no. 5, p. 412.

Zimmer, K., Zhang, Y.L., Lu, P., Chen, Y.Y., Zhang, G.R., Dalkilic, M. and Zhu, C., 2016, SUPCRTBL: A revised and extended thermodynamic dataset and software package of SUPCRT92: Computer and Geosciences, v. 90, p. 97–111.

Fluorite from Phosphate, MT. Courtesy of Michael J. Gobla.